chemistry

MDPI

Article

A Systematic Study of the Catalytic Decomposition Process of Ammonium Perchlorate and Its Decomposition Products Catalyzed by Copper and Copper Oxides

Guifeng Xiang [1,†], Xiaolin Tang [2,3,†], Chenhui Ma [1], Zeyu Zheng [3], Yifu Zhang [2,3,*] and Chi Huang [3,*]

[1] Hubei Space Jianghe Chemical Co., Ltd., Yichang 444200, China; xgfeng888@163.com (G.X.); mch12131@163.com (C.M.)
[2] Hubei Key Laboratory of Radiation Chemistry and Functional Materials, School of Nuclear Technology and Chemistry & Biology, Hubei University of Science and Technology, Xianning 437100, China; winters@whu.edu.cn
[3] College of Chemistry and Molecular Sciences, Wuhan University, Wuhan 430072, China; 2016301040200@whu.edu.cn
* Correspondence: yfzhang2023@whu.edu.cn (Y.Z.); chihuang@whu.edu.cn (C.H.)
† These authors contributed equally to this work.

Abstract

To reveal the core mechanism of copper-based materials in catalyzing ammonium perchlorate (AP) decomposition, three copper-based materials with the simplest structures (Cu, Cu_2O and CuO) are selected as research objects. This study systematically investigates their catalytic performances, gaseous product evolution, kinetic laws, and combustion behavior in AP decomposition. The results show that all three materials exhibit excellent catalytic activity, reducing the peak temperature of AP high-temperature decomposition to 325.1 °C, 329.9 °Cand 337.3 °C, respectively, with the catalytic activity order of Cu > Cu_2O > CuO. Gaseous product analysis confirms that both temperature and catalyst type jointly regulate product distribution. Kinetic analysis shows that the activation energy of Cu and Cu_2O catalytic processes exhibits a three-stage change of "increase-decrease-increase" (related to their own oxidation), while CuO shows a two-stage change, and the kinetic behaviors of the three are consistent in the later stage. Combustion experiments indicate that catalytic activity is positively correlated with combustion efficiency; the Cu-catalyzed system has the shortest combustion duration (383 ms) and the largest flame area. This study proposes the catalytic process of copper-based materials as "initial property regulation-unified active species (CuO) action", providing theoretical support for the directional design of high-performance copper-based catalysts.

Keywords: copper-based catalyst; ammonium perchlorate; catalytic performance; reaction mechanism; gaseous product

Check for updates

Academic Editor: Igor Alabugin

Received: 4 December 2025
Revised: 28 January 2026
Accepted: 11 February 2026
Published: 13 February 2026

Copyright: © 2026 by the authors. Licensee MDPI, Basel, Switzerland. This article is an open access article distributed under the terms and conditions of the Creative Commons Attribution (CC BY) license.

1. Introduction

Composite solid propellants (CSPs) serve as core power sources in aerospace propulsion and weapon launching, where their energy release efficiency and combustion stability directly determine the overall performance of equipment [1–4]. Ammonium Perchlorate (AP) has become the most widely used oxidizer in composite solid propellants (accounting for 60–90% of the total propellant mass) due to its high oxygen content (60.1%), appropriate density (1.95 g·cm^{-3}), and excellent chemical stability [5–7]. The thermal decomposition behavior of AP is the key to regulating propellant combustion

performance—its high-temperature decomposition (HTD) peak temperature typically exceeds 420 °C with a slow decomposition rate, leading to long ignition delay and low burning rate of propellants [8–10]. Therefore, developing high-efficiency catalysts to achieve low-temperature and rapid decomposition of AP is a core scientific issue and technical bottleneck for improving the comprehensive performance of composite solid propellants [2].

Among numerous catalysts for AP decomposition, copper-based catalysts have emerged as a research hotspot due to their outstanding advantages, including excellent catalytic activity, good environmental compatibility, low cost, and high safety [11–16]. Compared with traditional catalysts such as lead-based and chromium-based ones, the maximum allowable concentration of copper-based catalysts in the working area is 10–100 times higher, and they cause no significant pollution to the ecological environment after disposal, conforming to the development trend of "green propulsion" [17–20]. Copper and its oxides (Cu, Cu_2O and CuO), as the simplest active components of copper-based catalysts, are not only core active units of complex copper-based catalysts (e.g., supported and composite oxide catalysts) but also exhibit excellent catalytic performance for AP decomposition, making them ideal research models to reveal the intrinsic mechanism of copper-based catalysis [21–25]. Extensive research has been devoted to optimizing the catalytic performance of Cu, Cu_2O and CuO. Various morphologies of CuO (spherical, flower-like, cross-shaped) synthesized by the hydrothermal method reduce the peak temperature by 68–125 °C, highlighting the dominant role of specific surface area and active site exposure [26]. Cubic and derived Cu_2O morphologies can lower the peak temperature by 72.7–78.6 °C, expanding the morphology-activity correlation of copper-based catalysts [27–29]. Hu's team [30] prepared CuO/Cu_2O microsphere modified fluorinated carbon nanosheets, and the experiment proved that the material not only has good AP catalytic performance, but also can accelerate the combustion of Al powder. Sun's team [31] synthesized Al@AP/CuO core–shell structure for its decomposition and combustion performance, and the theoretical calculation results were combined to prove that the AP adsorption and conversion behavior on the CuO surface is the key to good catalytic and combustion behavior. Peng's group [32] prepared CuO microspheres with a particle size of about 1 μm using HKUST-1 as a precursor, which can reduce the decomposition peak temperature of AP from 424 °C to 338 °C.

Although it has been confirmed that copper-based catalysts (whose catalytic essence is Cu, Cu_2O, and CuO) have excellent catalytic effects, three core scientific questions have not yet been solved. Firstly, the differences in catalytic mechanisms among the three copper-based catalysts are not yet clear. Currently, most research focuses on improving the catalytic performance of copper-based catalysts and has achieved excellent research results [21–25]. However, there is a lack of systematic comparison of the catalytic behavior among the three catalysts, and the intrinsic correlation between physical and chemical properties (such as electron transfer ability and reducibility) and catalytic mechanisms has not been revealed. Secondly, the study confirmed the structure-activity relationship between the decomposition process and gaseous products. The gaseous products of AP decomposition (such as N_2O, NO_x, ClO_x) directly affect the combustion efficiency and exhaust emissions of propellants [33,34], and the regulation laws and mechanisms of the three catalysts on product composition have not been systematically reported. Thirdly, the correlation between catalytic kinetics and combustion performance is still unclear. Existing studies analyze catalytic decomposition or combustion processes in isolation, failing to establish a complete correlation chain, which hinders the directional design of catalysts.

To promote further research on related issues, it is necessary to fully consider other variables while studying the differences in catalytic mechanisms, catalytic products, and combustion of the three basic copper-based materials (Cu, Cu_2O, and CuO) in the catalytic

process, and speculate on the relationship between these differences and the physicochemical properties of the three materials. Efforts should be made to establish a connection between the properties and performance of copper-based catalysts, providing guidance for the structural design of copper-based catalysts with better performance in the future. Based on this idea, this article tested the decomposition temperature, decomposition product distribution, decomposition activation energy changes, and laser ignition combustion process of three catalysts catalyzing AP under the same conditions as much as possible, and combined DFT calculations to speculate the possible catalytic mechanism. The research results improve the basic theory of copper-based catalyzed AP decomposition and have important guiding value for the development of high-efficiency catalysts for composite solid propellants.

2. Materials and Methods

2.1. Materials and Their Characterizations

High-purity ammonium perchlorate (AP, NH4ClO4, Type II/Class 3) was bought from Tianyuan Chemical Co., Ltd. (Yancheng, China). Metallic copper (Cu), cuprous oxide (Cu2O) and copper oxides (CuO) powders were bought from Luoen Company (Wenzhou, China), and all raw materials were directly utilized without additional purification treatments. X-ray diffraction (XRD) measurements were performed on a Rigaku Smartlab 9 kW diffractometer (Tokyo, Japan), employing Cu Kα radiation (λ = 1.5406 Å) operated at 45 kV and 200 mA, with a scanning rate of 8° per minute.

2.2. Catalytic Characterizations

AP and each catalyst (Cu, Cu_2O, CuO) were accurately weighed and homogenously mixed with a catalyst mass fraction of 5% [33]. Thermogravimetry-Differential Scanning Calorimetry (TG-DSC) measurements were conducted to evaluate the catalytic performance of the samples, which enabled simultaneous monitoring of mass variation and heat absorption/release behaviors during the programmed heating process. TG-DSC tests were performed on a NETZSCH STA-2500 synchronous thermal analyzer (NETZSCH, Selb, Germany) with a temperature range of 30–500 °C and a heating rate of 10 °C per minute. All AP/catalyst composite samples were tested under a high-purity nitrogen atmosphere to prevent oxidative interference.

Isothermal experiments were carried out to investigate the physicochemical transformations of the reaction system at a fixed temperature. The specific protocol involved heating the sample to the target temperature at a rate of 10 °C per minute, followed by isothermal holding for a predetermined duration. Thermogravimetry-Fourier Transform Infrared Spectroscopy (TG-IR) measurements were employed to identify the gaseous decomposition products of AP/catalyst samples and perform relative quantitative analysis. The carrier gas flow rate was set to 20 $mL \cdot min^{-1}$ during the tests, and the infrared detection was conducted using a Thermo Fisher (Waltham, MA, USA) IS-50 Fourier transform infrared spectrometer. Gas composition calculation in detail is shown in Supplementary Materials (Table S1).

2.3. Combustion Tests

The combustion performance evaluations were conducted following the experimental protocol described in our previous work [35,36]. Specifically, a water-cooled CO_2 laser (Shanghai Yuhong Laser Equipment Co., Ltd., Shanghai, China) was employed to provide enough energy flux for sample ignition. The laser was operated at a power output of 80 W and a pulse duration of 2 s. Approximately 50 mg of each sample was loaded into an alumina (Al_2O_3) crucible for each test.

During the ignition and combustion processes, an AvaSpec-2048 fiber-optic spectrometer (Avantes BV, Apeldoorn, The Netherlands) was used to record the emission spectra with a spectral resolution of 0.8 nm. A Phantom M340 high-speed camera (Vision Research, Wayne, NJ, USA) was employed to capture the chemiluminescence signals at a frame rate of 1000 frames per second. Throughout the tests, high-purity nitrogen (N_2) was continuously injected into the combustion chamber to displace air, ensuring the samples burned in a 0.1 MPa N_2 atmosphere.

3. Results and Discussion

3.1. Catalytic Performance of Cu, Cu_2O and CuO in AP Decomposition

As the simplest copper-based materials, Cu, Cu_2O and CuO play a guiding role in the further development of copper-based catalysts by clarifying their catalytic mechanisms. In this study, these three materials were selected as research objects to systematically analyze the differences in their catalytic performance for AP decomposition and the underlying influencing factors. The test results in Figure 1a show that the XRD characteristic peaks of the three commercially available copper-based materials are basically consistent with the standard cards (Cu: 04-0836, Cu_2O: 34-1354, CuO: 45-0937), indicating high catalyst purity without obvious impurities. BET test results reveal slight differences in specific surface area among the three: CuO has the largest specific surface area, followed by Cu and Cu_2O (Figure S1). Their size distributions of the three materials are shown in Figure S2, and the results are in line with the BET. The difference in specific surface area is very small and can be essentially ignored, and its impact on catalytic activity can also be neglected. In addition, SEM tests were conducted on the three materials to observe their morphology, and the test results are shown in Figure S3. They show the size in nanoscale. XPS characterization results (Figure S4) further reveal the surface copper oxidation state characteristics of the three copper-based materials: the Cu $2p_3/_2$ main peak of the metallic Cu sample is located at ~932.6 eV, corresponding to the characteristic peak of Cu(0), and the satellite peaks of Cu^{2+} near 942 eV and 962 eV are extremely weak, indicating that only a small amount of oxidized species (Cu(I)/Cu(II)) generated by air exposure exist on its surface, while the main body remains in the metallic state; the Cu $2p_3/_2$ main peak of the Cu_2O sample is concentrated at ~932.4 eV, with no obvious characteristic satellite peaks of Cu^{2+}, confirming that the surface is mainly composed of Cu(I) without significant oxidative deterioration; the Cu $2p_3/_2$ main peak of the CuO sample is at ~934.6 eV, and strong satellite peaks appear near 942 eV and 962 eV, which are fully consistent with the XPS characteristics of Cu(II), indicating a uniform surface oxidation state and high purity. These results are consistent with the high-purity conclusion from XRD characterization, clarifying the initial surface oxidation state differences (Cu(0), Cu(I), Cu(II)) of the three materials. They provide a surface state basis for the subsequent oxidative conversion of Cu and Cu_2O to Cu(II) (CuO) during the catalytic process, further verifying the catalytic mechanism of "initial property regulation-unified active species (CuO) action". In a word, due to the different valence states of Cu in Cu, Cu_2O, and CuO, the shapes and sizes of their XPS spectral lines will vary. Therefore, XPS can be used to reflect the differences in chemical states of Cu among the three materials. From the tested XPS, it can be seen that the XPS of Cu in the three materials are different, indicating that there are differences in the chemical states of Cu on the surfaces of the three materials. It can be concluded that the surfaces of Cu and Cu_2O are different from those of CuO and have not been oxidized.

TG-DSC tests were performed on the mixed samples of Cu, Cu_2O, CuO with AP, and the results are shown in Figure 1b,c. All three materials exhibit excellent catalytic effects, significantly reducing the peak temperature of AP's high-temperature decomposition: Cu reduces the peak temperature to 325.1 °C, Cu_2O to 329.9 °C, and CuO to 337.3 °C, with the

catalytic activity order of Cu > Cu_2O > CuO. Compared with the pure AP with the peak temperature of 420.6 °C [36], Cu, Cu_2O and CuO reduce the peak temperature by 95.5 °C, 90.7 °C and 83.3 °C, respectively. Notably, the DSC curves all show exothermic peaks after the AP crystal transformation stage (approximately 240 °C), which is significantly different from the decomposition of pure AP [17]. The achieved performances are comparable to the previous works, as shown in Table S2. Combined with the XRD analysis of the residual products after the reaction in Figure 1d, it can be seen that both Cu and Cu_2O are oxidized to CuO during the reaction, indicating that all three materials ultimately exert their catalytic effects in the form of CuO. CuO has a strong adsorption capacity for AP decomposition intermediates, which can transfer the redox reactions originally occurring in the gas phase to the catalyst surface [4,28]. The heat released by the reaction is more easily detected by DSC, thus showing an overall exothermic characteristic. In addition, although the materials significantly accelerate the decomposition process, the DSC curves still show two decomposition peaks, indicating that AP still undergoes a two-stage decomposition process under the action of the three materials, suggesting a transition of the rate-determining step during the catalytic process.

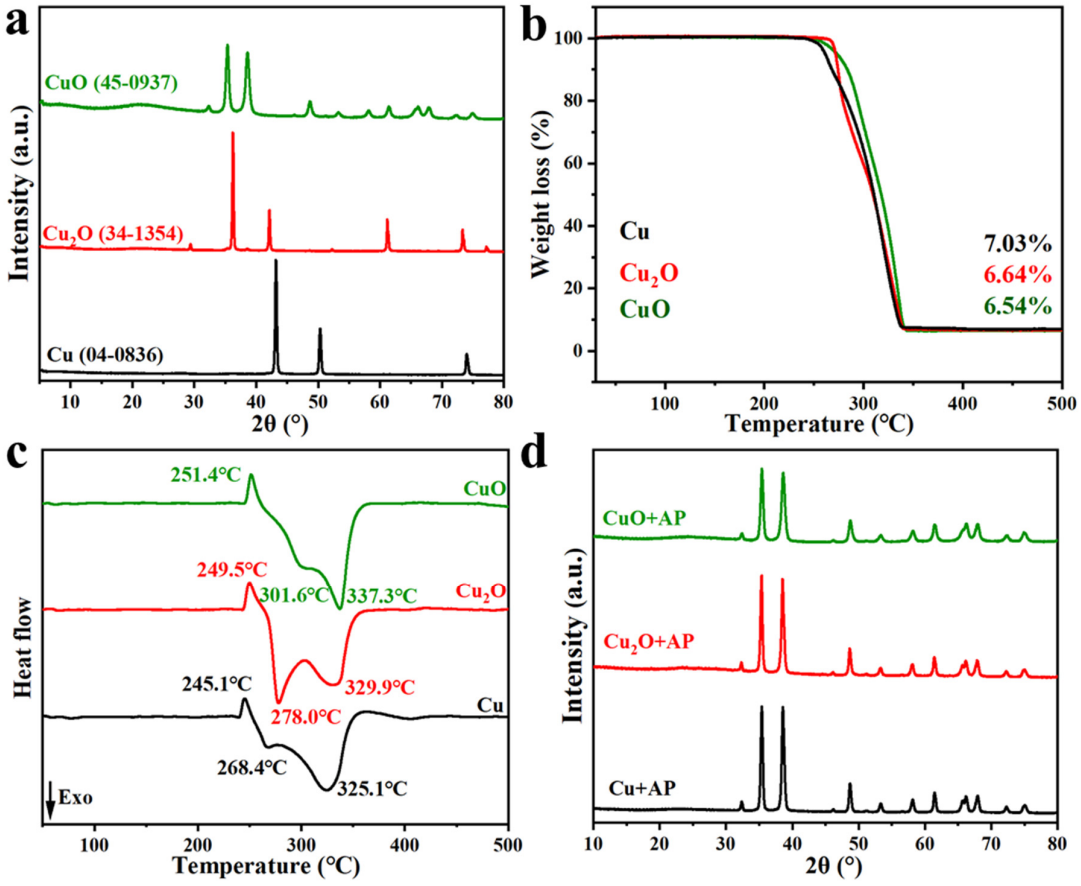


Figure 1. (**a**) XRD patterns of the three copper-based materials; (**b**,**c**) TG-DSC results of AP catalyzed by Cu, Cu_2O and CuO: (**b**) TG curves; (**c**) DSC curves; (**d**) XRD patterns of residual products after the AP decomposition catalyzed by Cu, Cu_2O and CuO.

By comparing and analyzing the catalytic behaviors of the three materials, it is found that their performance differences mainly stem from the differences in electron transfer capacity and reducibility. First, there are obvious differences in the initial decomposition temperature. The initial decomposition temperature of AP catalyzed by Cu and CuO is significantly earlier than that catalyzed by Cu_2O (Figure 1b), which is directly related to the electron transfer capacity of the three. Cu is a good conductor, while Cu_2O

and CuO are semiconductors. Moreover, the band gap of CuO (1.2–1.9 eV) is smaller than that of Cu_2O (2.0–2.9 eV) [37,38], resulting in the electron transfer capacity order of Cu > CuO > Cu_2O. The decomposition of pure AP is dominated by the proton transfer mechanism, and the electron transfer mechanism is difficult to occur [35]. Materials with electron transfer capacity can open the electron transfer channel and accelerate the initial decomposition [39]. Therefore, the difference in electron transfer capacity leads to the difference in initial decomposition temperature. Second, the initial decomposition rate follows the order of Cu ≈ Cu_2O > CuO. This difference is closely related to the reducibility of the materials. Cu and Cu_2O have strong reducibility. After the AP crystal transformation (before a large amount of $HClO_4$ is generated, no mass change is observed in TG and no endothermic/exothermic signal in DSC, indicating that the catalyst is not oxidized), they can undergo redox reactions with $HClO_4$ generated by AP decomposition: on the one hand, the released heat accelerates the temperature rise on the catalyst surface; on the other hand, it promotes the forward progress of the reversible reaction of AP decomposition into NH_3 and $HClO_4$, thereby accelerating the initial decomposition. In contrast, CuO has weak reducibility and cannot accelerate the initial decomposition through this pathway, resulting in a relatively slow initial decomposition rate. In a word, all three copper-based materials exhibit excellent catalytic performance for AP decomposition, but their catalytic behaviors are significantly different due to differences in electron transfer capacity and reducibility, and they all eventually convert to CuO to exert catalytic effects.

To further investigate the differences in catalytic performance of three copper-based materials towards AP at lower temperatures, isothermal tests were conducted on the mixed samples, and the results are shown in Figure 2. In the isothermal experiment, the catalytic activity order of the three materials is still Cu > Cu_2O > CuO, which is consistent with the TG-DSC test results, confirming the rationality of the catalytic behavior (Figure 2a). Meanwhile, Figure 2c,e show that the colors of Cu and Cu_2O change to black after the isothermal experiment. Combined with the XRD results, it can be confirmed that they have been converted to CuO, indicating that the conversion of Cu and Cu_2O to CuO can occur at relatively low temperatures, further supporting the previous speculation on the catalytic process.

3.2. Gaseous Product Analysis of AP Decomposition Catalyzed by Cu, Cu_2O and CuO

To clarify the effects of three materials on the decomposition gas products of AP, TG-IR testing was used to qualitatively analyze the decomposition gas and semi-quantitatively analyze the NH_3 oxidation gas. The semi-quantitative analysis process has been explained in SI, and the purpose of this method is to compare and analyze the gas products of different catalysts. Its accuracy is relatively limited, and combined with theoretical calculations, it reveals the inherent relationship between the evolution law of gas products and the catalytic mechanism. The analysis results of the gaseous products of copper-catalysed AP decomposition are shown in Figure 3. The gas signal is detected at 21.5 min, which is significantly earlier than that of pure AP [36], consistent with the excellent electron transfer capacity of Cu that accelerates the initial decomposition. Only the N_2O signal appears in the IR spectrum at the initial stage, which is presumably because Cu, as a reducing agent, is first oxidized by active oxygen, and the initial decomposition products of AP remain unchanged. The NO_2 signal is detected at approximately 22.5 min, which is 1.2 min earlier than that of pure AP. This is related to the adsorption and conversion of intermediates by Cu after being converted to CuO: the adsorption capacity of CuO for AP decomposition intermediates enables the redox reaction between NH_3 (reductive) and $HClO_4$ derivatives (oxidative) to occur on the catalyst surface, providing favorable conditions for the formation of NO_2. Due to the low temperature in the initial stage, the oxidation reaction rate is slow,

and N_2O is accounting for 33.8%. With the increase in temperature, the release rate of $HClO_4$ accelerates and the oxidation reaction speeds up, leading to an enhanced oxidation degree of NH_3. The proportion of N_2 reaches 45.5%, NO_2 accounts for 13.5%, while the proportions of NO and NOCl are only 2.1% and 5.1%, respectively (Figure 3d). Overall, N_2 and N_2O remain the main products.

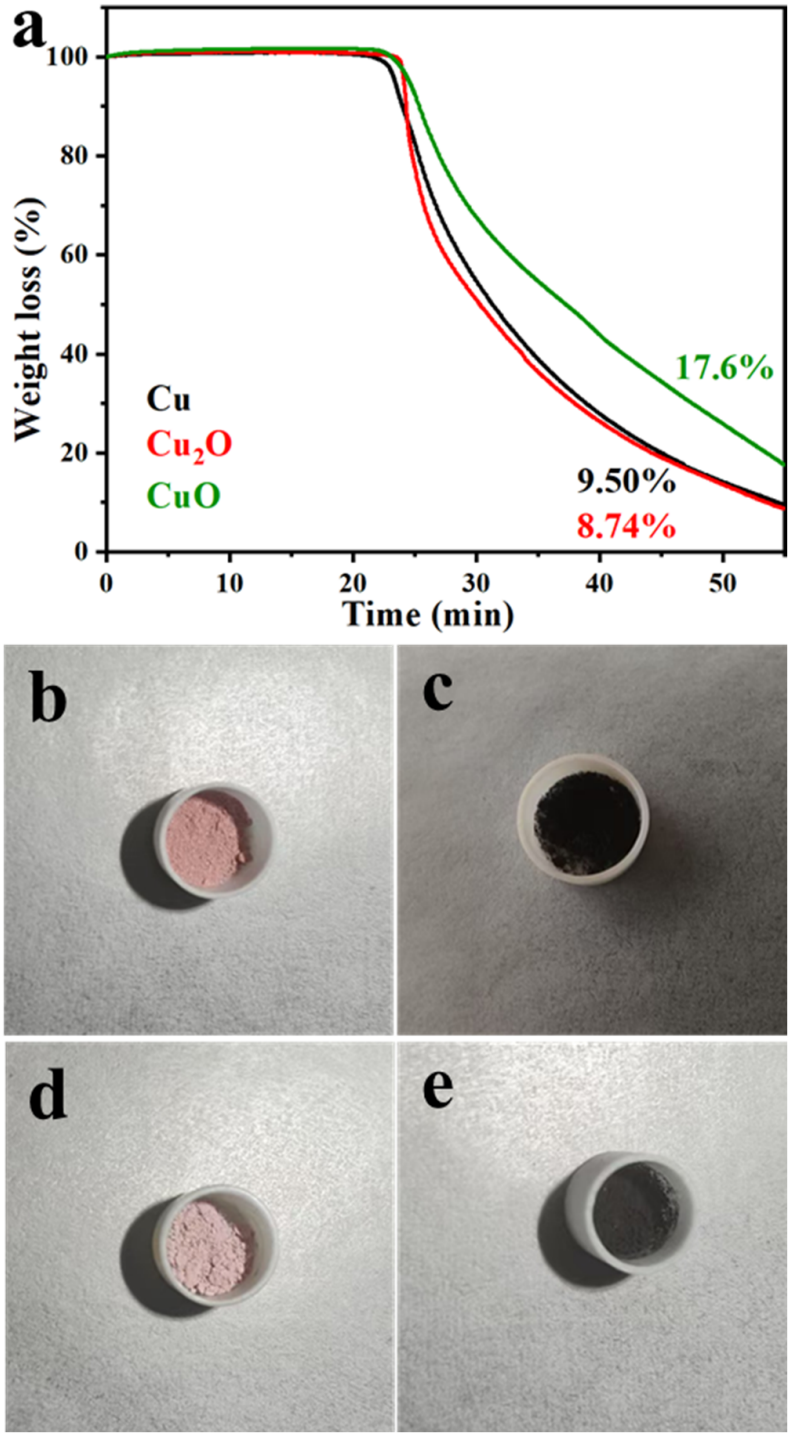


Figure 2. (**a**) TG results of AP catalyzed by Cu, Cu_2O, and CuO in isothermal experiments; (**b**–**e**) Photos of crucibles before and after isothermal experiments for Cu and Cu_2O: (**b**) Cu before isothermal treatment; (**c**) Cu after isothermal treatment; (**d**) Cu_2O before isothermal treatment; (**e**) Cu_2O after isothermal treatment.

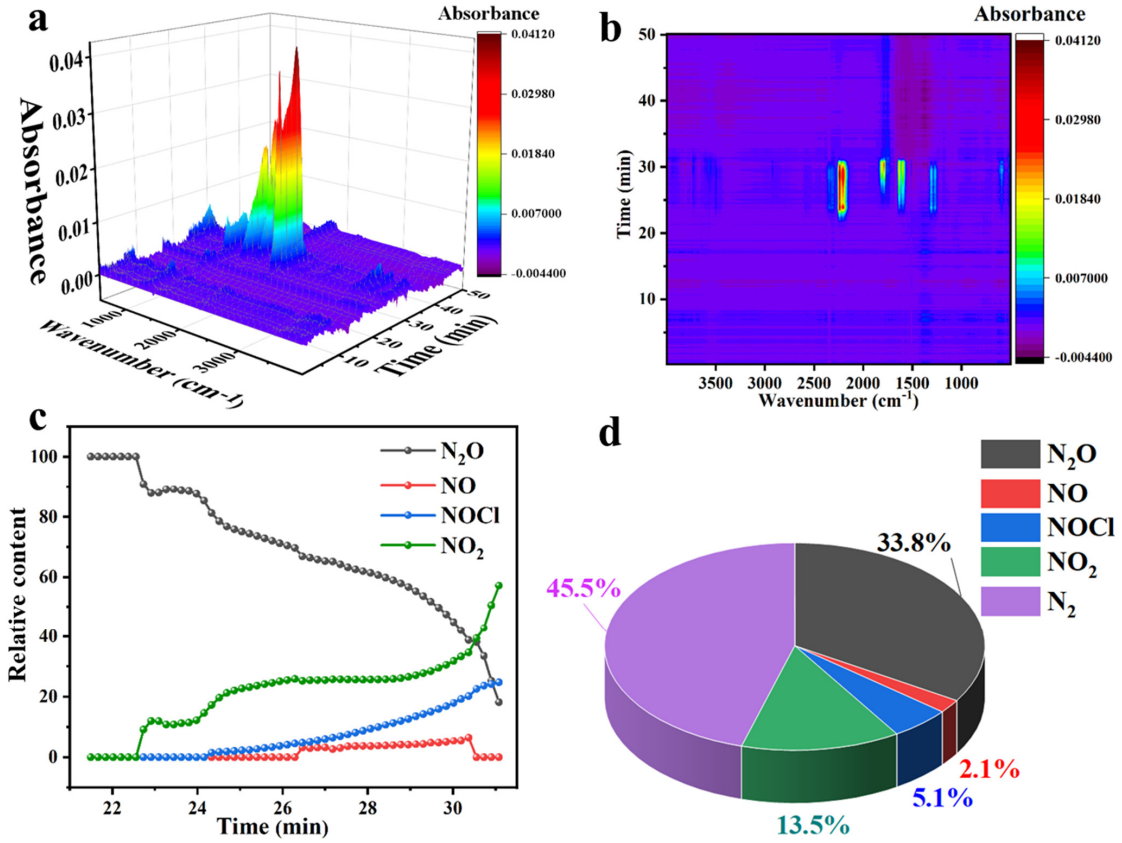


Figure 3. Gaseous product analysis results of AP decomposition catalyzed by Cu: (**a**) TG-IR 3D plot; (**b**) TG-IR contour plot; (**c**) Time-dependent relative content of various gases in TG-IR; (**d**) Total gas release proportion.

The release law of gaseous products from AP decomposition catalyzed by Cu_2O is highly similar to that catalyzed by Cu (Figure 4), which is consistent with their similar catalytic processes—both are first oxidized to CuO before exerting catalytic effects. A large amount of NO_2 is also detected at the end of the reaction, further confirming that the formation of NO_2 is positively correlated with temperature. However, in terms of total gas proportion, the proportion of N_2 in the products catalyzed by Cu_2O reaches 61.1%, which is higher than that in the Cu-catalyzed system (45.5%), while the proportion of N_2O is 25.2%, lower than that in the Cu-catalyzed system. This difference originates from the faster initial decomposition rate of Cu_2O: a large amount of AP decomposes at relatively low temperatures, and the oxidation reaction rate is limited at this time, so the decomposition products of AP are mainly N_2, resulting in a significantly higher overall proportion of N_2.

The analysis results of gaseous products from AP decomposition catalyzed by CuO are shown in Figure 5. N_2O is also the initial decomposition product, indicating that CuO only accelerates AP decomposition through electron transfer capacity in the low-temperature stage without changing the type of gaseous products. With the increase in temperature, signals of NO, NOCl, and NO_2 are detected successively, which is consistent with the mechanism of the Cu and Cu_2O catalytic systems. Due to the highest peak temperature of AP decomposition catalyzed by CuO, the oxidation degree of NH_3 is significantly enhanced. The instantaneous proportion of NO_2 exceeds 50% in the late stage of the reaction, and the total proportion of NO and its derivatives (NO, NOCl, NO_2) in the total gas reaches 34.8%, which is higher than that in the Cu (20.7%) and Cu_2O (13.7%) catalytic systems. This confirms the speculation that "the higher the temperature, the higher the proportion of NO and its derivatives".

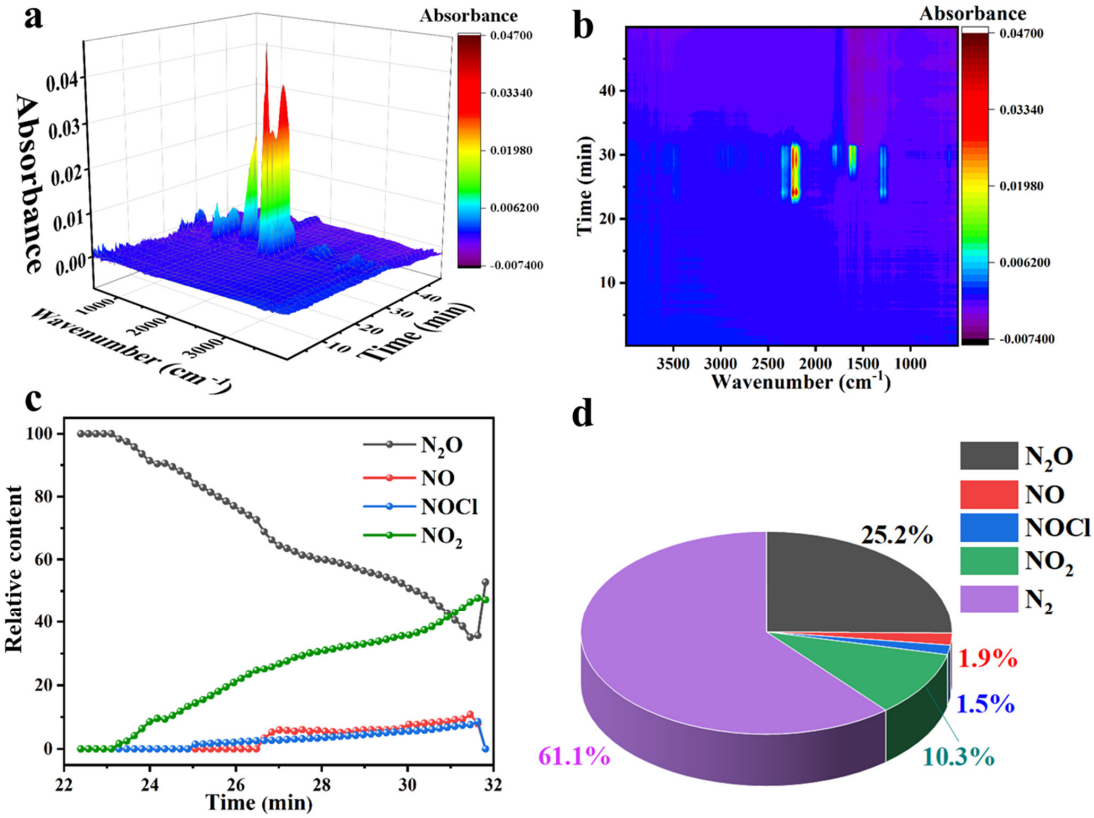


Figure 4. Gaseous product analysis results of AP decomposition catalyzed by Cu_2O: (**a**) TG-IR 3D plot; (**b**) TG-IR contour plot; (**c**) Time-dependent relative content of various gases in TG-IR; (**d**) Total gas release proportion.

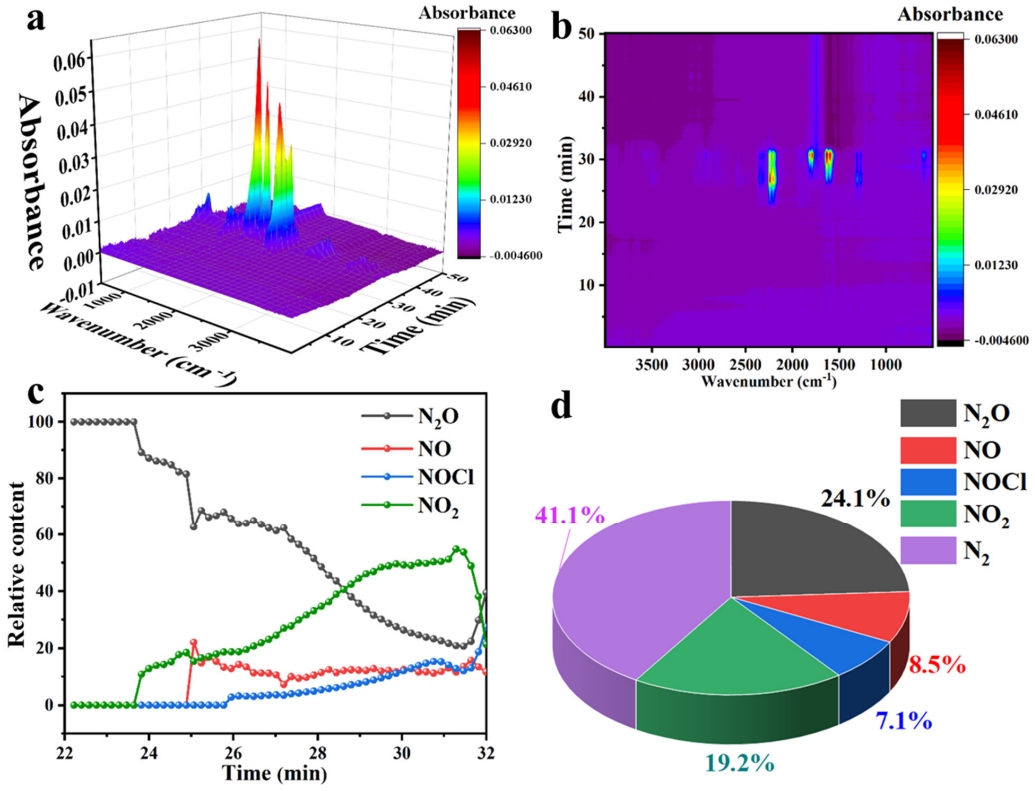


Figure 5. Gaseous product analysis results of AP decomposition catalyzed by CuO: (**a**) TG-IR 3D plot; (**b**) TG-IR contour plot; (**c**) Time-dependent relative content of various gases in TG-IR; (**d**) Total gas release proportion.

To theoretically verify the adsorption and conversion mechanism of CuO on AP decomposition intermediates, density functional theory (DFT) calculations were performed to investigate the adsorption behavior of the CuO (111) crystal plane on NH_3 and $HClO_4$, and the results are shown in Figure 6. The adsorption energy of the CuO (111) crystal plane for NH_3 is −0.62 eV, and for $HClO_4$ is −1.55 eV, indicating that both intermediates can be adsorbed on the CuO surface, and the adsorption capacity for $HClO_4$ is stronger. The electron cloud density diagram shows that the structural stability of $HClO_4$ decreases after adsorption (Figure 6c,d), making it prone to decomposition and generating active oxygen. The active oxygen further oxidizes NH_3 to form nitrogen oxides with different valences (Figure 6e,f). This calculation result is consistent with the phenomenon in the TG-IR test that "the content of high-valent nitrogen oxides increases with the increase in temperature", clarifying the adsorption-decomposition-oxidation mechanism of CuO on intermediates. In a word, in the catalytic AP reaction, $HClO_4$ adsorbs on the surface of CuO and subsequently decomposes to generate active oxygen species for the NH_3 oxidation process. As the temperature increases, this process accelerates further, the content of active oxygen species increases, and the degree of NH_3 oxidation further increases.

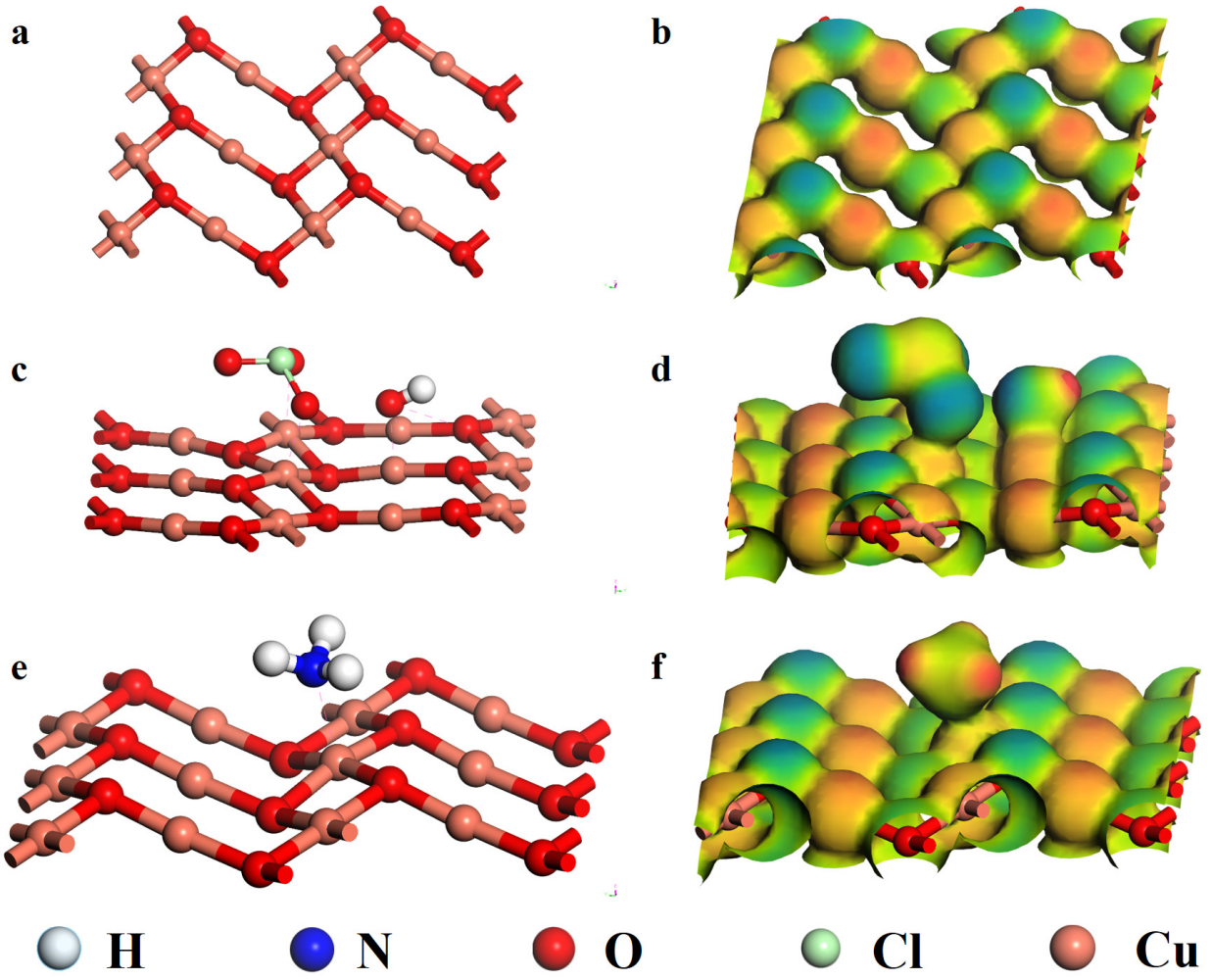


Figure 6. Adsorption of AP decomposition intermediates on CuO: (**a**) CuO (111); (**b**) Electron cloud density of CuO (111); (**c**) CuO (111) + $HClO_4$; (**d**) Electron cloud density of CuO (111) + $HClO_4$; (**e**) CuO (111) + NH_3; (**f**) Electron cloud density of CuO (111) + NH_3.

To further explore the product differences in the three materials under low-temperature conditions, isothermal TG-IR tests were conducted, and the results are shown in Figure 7. In

the Cu-catalyzed system (Figure 7a,b), the N_2O peak dominates in the initial stage. With the extension of isothermal time, the N_2O peak gradually weakens, while the peaks of NO_2 and NOCl strengthen. In the late stage of the reaction, the contents of NO_2 and NOCl exceed those of N_2O, a phenomenon not observed in the temperature-ramping experiment. Two reasons are speculated: first, the decomposition rate is slow in the isothermal experiment, allowing NH_3 to be fully oxidized at the Cu active sites; second, the exothermic redox reaction on the Cu surface forms local hot spots, accelerating the oxidation reaction. The gas variation law of the Cu_2O-catalyzed system (Figure 7c,d) is basically consistent with that of the Cu-catalyzed system, except that the relative content of N_2O is higher in the initial stage. In the CuO-catalyzed system (Figure 7e,f), the initial gas release amount is small, and the gradual enhancement of the NO_2 peak with isothermal time can be clearly observed. Since the number of Cu active sites remains unchanged, this further confirms that the existence of local hot spots accelerates the oxidation of NH_3.

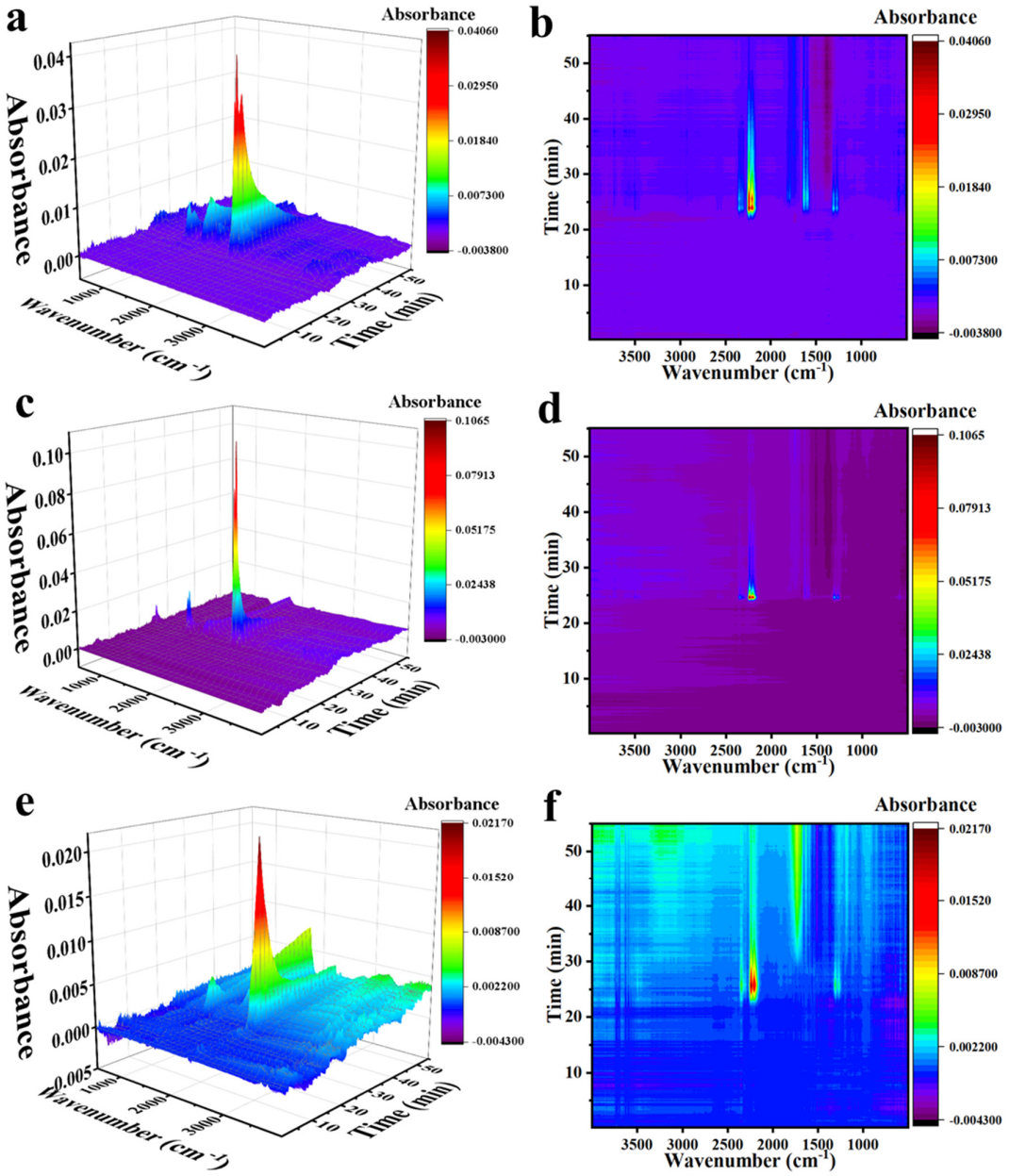


Figure 7. TG-IR results of isothermal experiments: (**a**,**b**) AP catalyzed by Cu; (**c**,**d**) AP catalyzed by Cu_2O; (**e**,**f**) AP catalyzed by CuO ((**a**,**c**,**e**) are TG-IR 3D plots; (**b**,**d**,**f**) are TG-IR contour plots).

3.3. Kinetic Study of AP Decomposition Catalyzed by Cu, Cu_2O and CuO

To clarify the effect of the three materials on the kinetics of AP decomposition, TG data under different heating rates were tested, and the activation energy was calculated using the Ozawa method [40]. The results are shown in Figure 8 and Figure S4. The heating rate has no significant effect on the catalytic mechanisms of the three materials, ensuring the reliability of the activation energy calculation. The activation energy curve of AP decomposition catalyzed by Cu shows a three-stage change of "increase-decrease-increase" (Figure 8b), which is significantly different from the two-stage change in pure AP [36]. Based on the test results and the relevant definition of activation energy, we speculate that the trend of activation energy changes is related to the rate determining steps or reaction pathways during the reaction process. Therefore, we propose follow-up ideas based on this data. Unfortunately, the details of this reaction process are currently difficult to capture, so this hypothesis has not been fully proven. In the first stage (α = 0.1–0.3), the activation energy increases, corresponding to the oxidation process of Cu to CuO: the rate-determining step gradually changes from the oxidation of Cu consuming $HClO_4$ to the decomposition of AP into NH_3 and $HClO_4$, and the energy required for the oxidation reaction leads to the increase in activation energy. In the second stage (α = 0.3–0.6), the activation energy decreases, and the minimum point corresponds to the part where the decomposition rate slows down in the TG curve, which is related to the adsorption.

Saturation on the AP particle surface, and the rate-determining step changes to the desorption process of intermediates. In the third stage (α = 0.6–0.9), the activation energy increases again. At this time, Cu has been completely converted to CuO, and the rate-determining step becomes the adsorption, conversion, and desorption of intermediates at the active sites of CuO. The increase in temperature intensifies the oxidation reaction, leading to the increase in activation energy, which also explains the enhanced oxidation degree of NH_3 at high temperatures. The activation energy curve of AP decomposition catalyzed by Cu_2O also shows a three-stage change (Figure 8d), consistent with the Cu-catalyzed system, confirming their similar catalytic mechanisms. The only difference is the α value corresponding to the minimum activation energy, which is related to the faster initial decomposition rate of Cu_2O and more weight loss in the early stage, resulting in an earlier α value for adsorption saturation. The activation energy curve of AP decomposition catalyzed by CuO only shows a two-stage change (Figure 8f), lacking the initial increasing stage, which further confirms that the initial increase in activation energy is related to the oxidation of the catalyst itself. Its curve trend is consistent with the latter two stages of the Cu and Cu_2O catalytic systems, indicating that after Cu and Cu_2O are oxidized to CuO, their catalytic kinetic behaviors are consistent with pure CuO, which once again verifies the conclusion that all three materials ultimately exert catalytic effects in the form of CuO.

Based on the above tests, we have speculated on the catalytic mechanism based on relevant research results and test data from this work (there is currently no direct evidence to prove it). Overall, in the first stage of Cu and Cu_2O, the oxidation process of Cu and Cu_2O is the rate-determining step of the reaction. In addition, the physical and chemical processes that occur also include the decomposition of AP into NH_3 and $HClO_4$ through electron (only Cu) or proton transfer, as well as their desorption on the AP surface and adsorption on the catalyst surface, and subsequent redox reactions. In the first stage of Cu and Cu_2O, which is also equivalent to the first stage of CuO, the desorption of NH_3 and $HClO_4$ on the surface of AP gradually becomes the determining step. At the same time, the decomposition of AP and subsequent oxidation-reduction reactions on the catalyst surface and gas phase are still occurring. In the final stage, the desorption process significantly accelerates, and the decomposition process of AP becomes the determining step. Subsequent redox reactions still occur widely in the gas phase and catalyst surface.

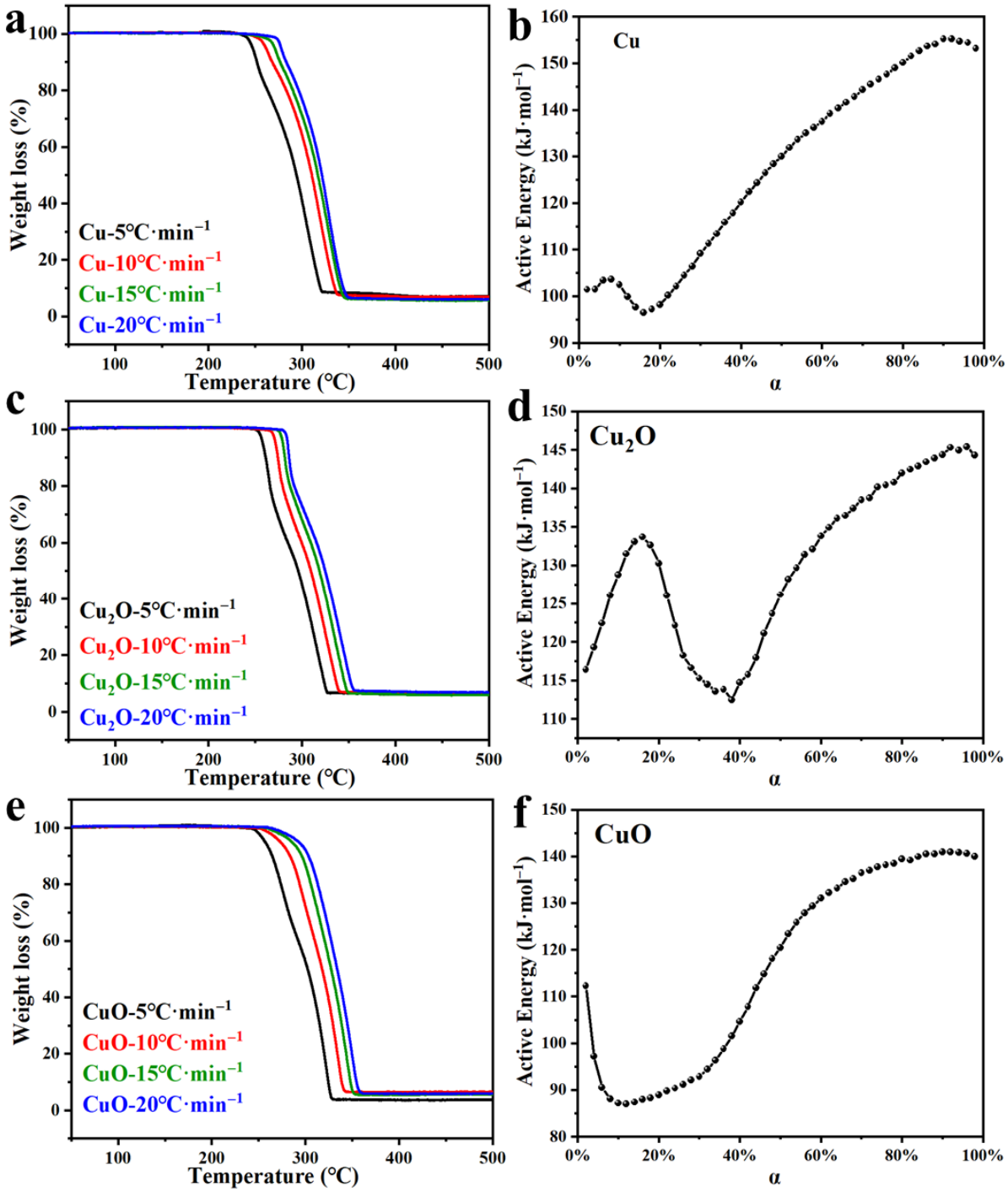


Figure 8. Kinetic calculation results of AP decomposition catalyzed by different materials: (**a**,**b**) AP catalyzed by Cu: (**a**) TG results under different heating rates; (**b**) Activation energy vs. reaction conversion degree; (**c**,**d**) AP catalyzed by Cu_2O: (**c**) TG results under different heating rates; (**d**) Activation energy vs. reaction conversion degree; (**e**,**f**) AP catalyzed by CuO: (**e**) TG results under different heating rates; (**f**) Activation energy vs. reaction conversion degree.

In addition, to verify the accuracy of the Ozawa method in calculating the variation in activation energy, we used another iso-conversional method, the Vyazovkin method, for supplementary calculations [41]. The calculated trend of activation energy variation is shown in Figure S5. There is indeed a difference in the activation energy values calculated by the two methods, but the change pattern of activation energy and the location of extreme points are basically the same. Therefore, it can be considered that the activation energy

change pattern calculated in this article is reliable and independent of the activation energy calculation method.

3.4. Combustion Performance of AP Catalyzed by Cu, Cu_2O and CuO

To explore the effect of the three materials on the AP combustion process, combustion experiments were conducted using laser ignition combined with high-speed photography technology [35], and the results are shown in Figures 9–11, respectively. It should be noted that the combustion duration is affected by factors such as particle packing mode, resulting in limited repeatability. The focus of the analysis is on the common characteristics of the combustion process. The combustion duration of AP catalyzed by Cu is 383 ms (Figure 9). Compared with pure AP [36], the combustion process has two significant differences: first, the flame area is significantly larger. This is because Cu accelerates AP decomposition, increasing the generation and diffusion rates of gas, thereby expanding the range of gas-phase redox reactions; second, the flame brightness changes from bright yellow-green (pure AP) to dark yellow. There are two possible reasons: on one hand, Cu promotes the reaction of intermediates on the catalyst surface, weakening the gas-phase reaction; on the other hand, Cu accelerates the release of active oxygen from $HClO_4$, enhancing the oxidation degree of the gas phase, converting the reducing flame to an oxidizing flame, and obvious outer flame structure appears at the flame edge. In addition, a white flame core is observed during the combustion process (Figure 9b,c), which is presumably caused by the incompletely reacted active intermediates generated by the rapid decomposition of AP. Some samples continue to burn after being ejected from the crucible, with very little residue, confirming that Cu can improve the combustion efficiency of AP.

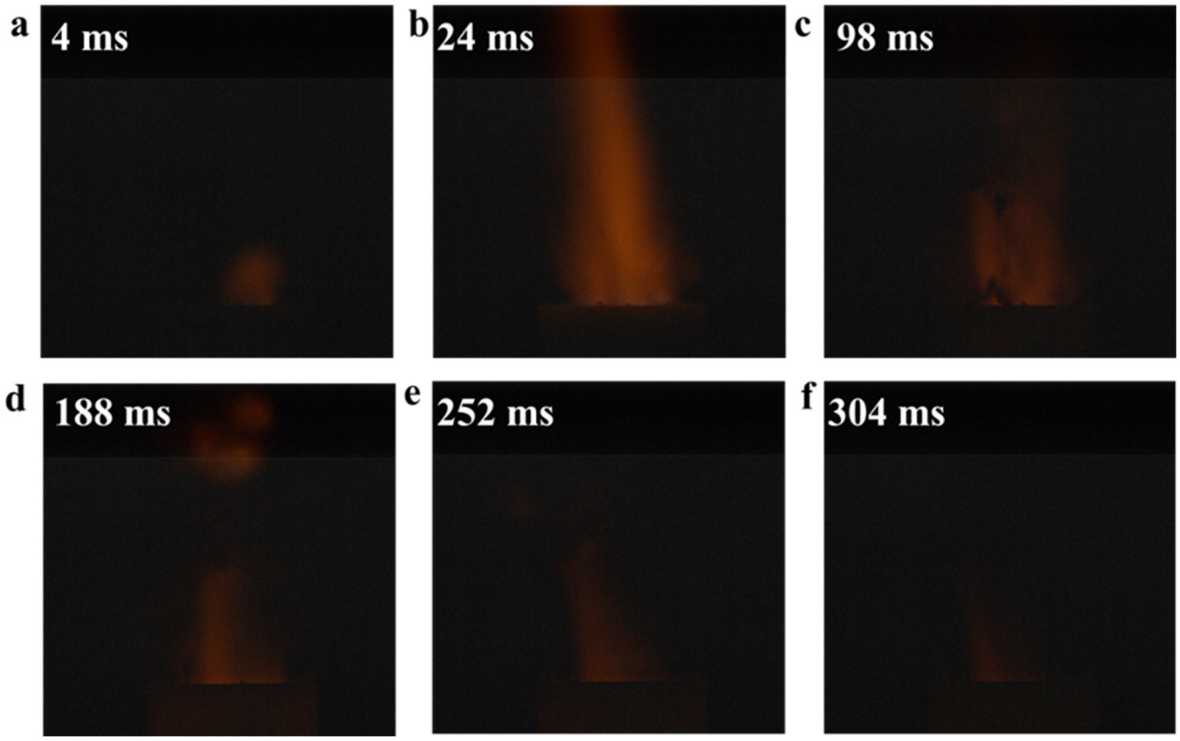


Figure 9. Combustion process of AP catalyzed by Cu (different time points): (**a**) 4 ms; (**b**) 24 ms; (**c**) 98 ms; (**d**) 188 ms; (**e**) 252 ms; (**f**) 304 ms.

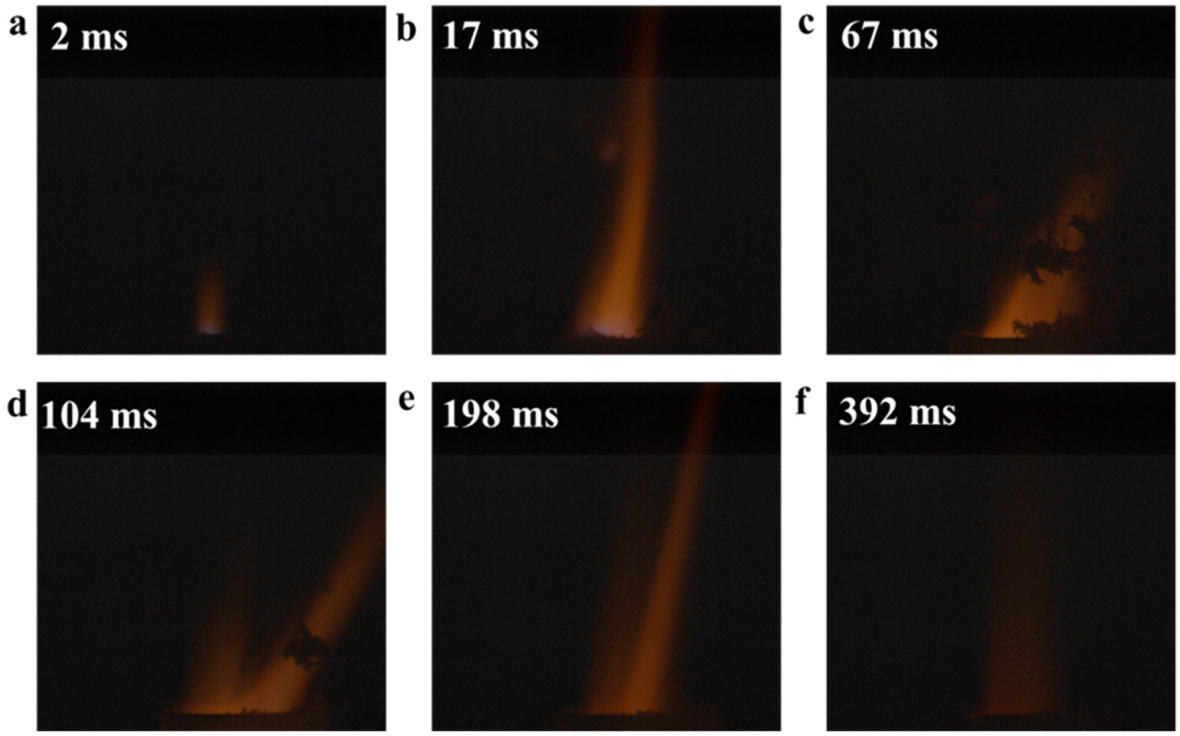


Figure 10. Combustion process of AP catalyzed by Cu_2O (different time points): (**a**) 2 ms; (**b**) 17 ms; (**c**) 67 ms; (**d**) 104 ms; (**e**) 198 ms; (**f**) 392 ms.

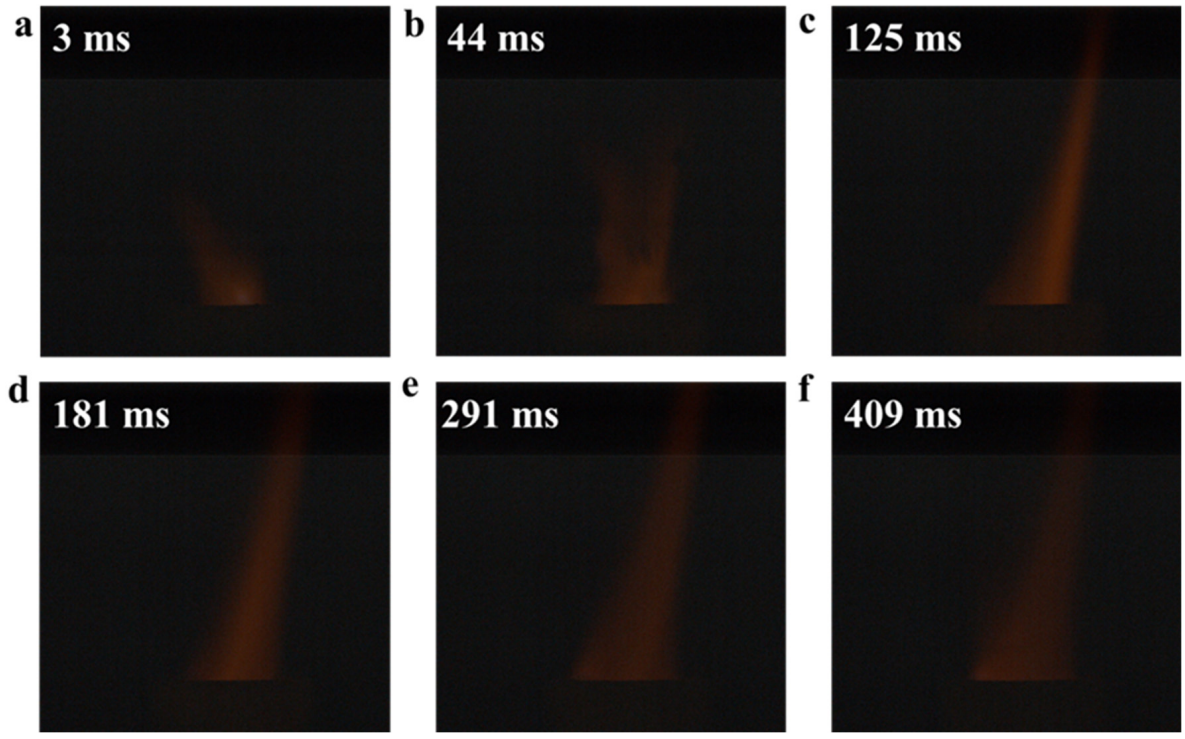


Figure 11. Combustion process of AP catalyzed by CuO (different time points): (**a**) 3 ms; (**b**) 44 ms; (**c**) 125 ms; (**d**) 181 ms; (**e**) 291 ms; (**f**) 409 ms.

The combustion duration of AP catalyzed by Cu_2O is 424 ms (Figure 10). The combustion process and flame structure are basically consistent with the Cu-catalyzed system. The flame is also dark yellow with a white flame core, and the samples continue to burn after

being ejected. This further confirms that Cu and Cu_2O have similar catalytic mechanisms, both accelerating AP decomposition and combustion through oxidation to CuO.

The combustion duration of AP catalyzed by CuO is 517 ms (Figure 11). The flame remains dark yellow throughout the combustion process, and there is no violent combustion stage observed in the Cu and Cu_2O catalytic systems. This difference originates from the lack of reducibility of CuO, which cannot accelerate the initial decomposition by consuming $HClO_4$ through redox reactions. The gas release rate is relatively gentle, resulting in a more stable combustion process, which once again confirms the correlation between the decomposition process and the combustion process.

The differences in combustion performance of the three copper-based materials are directly related to their catalytic mechanisms. A unified catalytic process can be summarized: Cu (good conductor + reducibility) and Cu_2O (reducibility) first accelerate the initial decomposition through electron transfer or redox reactions, and then are oxidized to CuO; CuO (semiconductor) accelerates decomposition through electron transfer in the low-temperature stage and accelerates the reaction through adsorption-conversion of intermediates in the high-temperature stage. This process provides a clear direction for the structural design of copper-based materials: copper-based materials with both excellent electron transfer capacity and reducibility are expected to exhibit better catalytic performance.

4. Conclusions

In conclusion, this work takes three basic copper-based materials (Cu, Cu_2O, and CuO) as research objects, and systematically clarifies their catalytic performance differences in AP decomposition through multi-dimensional characterizations and performance tests. The key conclusions are as follows: (1) All three copper-based materials exhibit excellent catalytic activity for AP decomposition, and their catalytic performance follows a consistent order of Cu > Cu_2O > CuO. Specifically, Cu, Cu_2O, and CuO reduce the peak temperature of AP high-temperature decomposition from 420.6 °C (pure AP) to 325.1 °C, 329.9 °C, and 337.3 °C, with temperature reductions of 95.5 °C, 90.7 °C, and 83.3 °C, respectively. (2) The catalytic process of the three materials follows a unified mechanism of "initial property regulation-unified active species action". Cu (a good conductor) and CuO (a narrow-bandgap semiconductor) have stronger electron transfer capabilities (in the order of Cu > CuO > Cu_2O), which can open the electron transfer channel for AP decomposition and significantly advance the initial decomposition temperature. Cu and Cu_2O, with strong reducibility, can react with $HClO_4$ generated in the initial stage of AP decomposition through redox reactions, accelerating the initial decomposition rate (Cu ≈ Cu_2O > CuO). In the medium- and high-temperature stages of the reaction, both Cu and Cu_2O are completely oxidized to CuO. Finally, the three materials exert their catalytic effects through the unified active species CuO, which reduces the decomposition peak temperature by adsorbing AP intermediates (NH_3 and $HClO_4$) and mediating surface redox reactions. (3) The correlation law of "catalyst type-temperature-gaseous product composition" was revealed. In the initial decomposition stage, N_2O is the main product of all three catalytic systems. As the temperature rises, the oxidation reaction of NH_3 mediated by CuO intensifies, leading to an increase in the proportion of high-valent nitrogen oxides such as NO, NOCl, and NO_2. The proportion of such products in the CuO-catalyzed system reaches 34.8%, which is significantly higher than that in the Cu (20.7%) and Cu_2O (13.7%) systems. Isothermal TG-IR tests further confirm that the local hot spot effect can accelerate NH_3 oxidation, enabling the formation of high-valent nitrogen oxides even under low-temperature isothermal conditions. DFT calculations verify that the CuO (111) crystal plane has a strong adsorption capacity for $HClO_4$ (adsorption energy: −1.55 eV). After adsorption, the structural stability of $HClO_4$ decreases, and it is prone to decomposition to generate active oxygen, providing

thermodynamic conditions for NH_3 oxidation. (4) Both catalytic kinetics and combustion performance are directly related to the catalytic mechanism. Due to their own oxidation process, the activation energy curves of Cu and Cu_2O catalytic processes show a three-stage change of "increase-decrease-increase", which is consistent with the adsorption saturation process. CuO has no initial oxidation step, so its activation energy shows a two-stage change, and its kinetic behavior is highly consistent with that of Cu and Cu_2O after they are oxidized to CuO. Combustion performance tests show that catalytic activity is positively correlated with combustion efficiency. The Cu-catalyzed system has the shortest combustion duration (383 ms) and the largest flame area, while the CuO system has the most stable combustion process (duration: 517 ms), which confirms the regulatory effect of initial decomposition rate on the combustion process. The research results improve the basic theory of copper-based catalyzed AP decomposition and have important guiding value for the development of high-efficiency materials for composite solid propellants.

Supplementary Materials: The following supporting information can be downloaded at: https://www.mdpi.com/article/10.3390/chemistry8020025/s1, Section S1. Gas Composition Calculation, including Table S1. Correction factor for main gas products of ammonia oxidation; Section S2. Activation Energy Calculation; Section S3. Supplementary Figures (Figure S1. Nitrogen adsorption–desorption isotherms of the three materials. Figure S2. The size distributions of the three materials. Figure S3. SEM images of three catalysts: (a) Cu; (b) Cu_2O; (c) CuO; Figure S4. XPS spectra of (a) Cu; (b) Cu_2O; (c) CuO; Figure S5. DTG diagrams tested at different heating rates: (a) Cu; (b) Cu_2O; (c) CuO; Figure S6. Changes in activation energy of three catalysts calculated using Vyazovkin method: (a) Cu; (b) Cu_2O; (c) CuO); Section S4. Supplementary Table (Table S2. Performance of this work compared with the previously reported materials. Section S5. References [11,18,40–48] are cited in the Supplementary Materials).

Author Contributions: Conceptualization, G.X. and X.T.; methodology, G.X. and X.T.; software, C.M. and Y.Z.; validation, G.X., X.T. and Z.Z.; formal analysis, G.X., X.T. and C.M.; investigation, G.X. and X.T.; resources, G.X. and X.T.; data curation, G.X., X.T. and Z.Z.; writing—original draft preparation, G.X., X.T. and Z.Z.; writing—review and editing, Y.Z. and C.H.; visualization, Z.Z.; supervision, Y.Z. and C.H.; project administration, C.H.; funding acquisition, C.H. All authors have read and agreed to the published version of the manuscript.

Funding: This research received no external funding.

Data Availability Statement: Data will be made available on request.

Acknowledgments: We thank the Core Research Facilities of College of Chemistry and Molecular Sciences at Wuhan University for the SEM and TEM characterization. In addition, we thank the Core Facility of Wuhan University for EDS characterization.

Conflicts of Interest: Authors Guifeng Xiang and Chenhui Ma were employed by the company Hubei Space Jianghe Chemical Co., Ltd. The remaining authors declare that the research was conducted in the absence of any commercial or financial relationships that could be construed as a potential conflict of interest.

References

1. Zhou, P.; Zhang, S.; Ren, Z.; Tang, X.; Zhang, K.; Zhou, R.; Wu, D.; Liao, J.; Zhang, Y.; Huang, C. In Situ Cutting of Ammonium Perchlorate Particles by Co-Bipy "scalpel" for High Efficiency Thermal Decomposition. *Adv. Sci.* **2022**, *9*, 2204109. [CrossRef]
2. Zhou, P.; Ren, Z.; Tang, X.; Zheng, Z.; Zhang, K.; Liao, J.; Zhong, Y.; Zhang, Y.; Huang, C. Interaction Between Prussian Blue Ultrathin Nanosheet and Ammonium Perchlorate for Highly Efficient Thermal Decomposition. *Adv. Funct. Mater.* **2023**, *33*, 2300661. [CrossRef]
3. Xu, R.; Xue, Z.; Yang, D.; Li, X.; Nie, H.; Guo, Y.; Guo, H.; Yan, Q.-L.; Gu, J. Highly Energy Release of Aluminum@Ammonium Perchlorate Composites Incorporated with Graphene Oxide-based Energetic Coordination Polymer. *Adv. Funct. Mater.* **2025**, *35*, 2423205. [CrossRef]

4. Zhang, M.; Wang, S.; Wang, X.-Y.; Wu, Z.-P.; Ding, B.-S.; Yang, L.; Tong, W.-C.; Ma, Q.; Wang, Q.-Y. Single Cu Atoms Anchored Energetic COFs as Combustion Catalytic Promoters toward Rapid and Concentrated Thermal Decomposition of Ammonium Perchlorate. *Adv. Sci.* **2025**, *12*, e01761. [CrossRef] [PubMed]
5. Hao, G.; Yang, R.; Kou, Y.; Wei, J.; Lu, Q.; Zhang, W.; Gao, H.; Zhao, F.; Jiang, W. Highly dispersed core–shell AP@AO energetic composites with good inhibitory effect on the low-temperature decomposition of AP and the burning rate of AP-based composite propellants. *Fuel* **2025**, *402*, 135967. [CrossRef]
6. Shi, J.; Xing, X.; Wang, H.; Ge, L.; Sun, H.; Lv, B. Oxygen vacancy enriched Cu-WO_3 hierarchical structures for the thermal decomposition of ammonium perchlorate. *Inorg. Chem. Front.* **2022**, *9*, 136–145. [CrossRef]
7. Yu, J.; Kou, Y.; Lei, H.; Lu, Q.; Xiao, L.; Yang, H.; Xu, X.; Yang, J.; Jiang, W.; Hao, G. Efficiently Constructed Core-Shelled Structured AP-Based Composites with Excellent Balance of High Energy Release and Low Sensitivity. *Small* **2025**, *21*, 2500967. [CrossRef]
8. Zhou, P.; Zhang, S.; Ren, Z.; Wang, Y.; Zhang, Y.; Huang, C. Study on the thermal decomposition behavior of ammonium perchlorate catalyzed by Zn–Co cooperation in MOF. *Inorg. Chem. Front.* **2022**, *9*, 5195–5209. [CrossRef]
9. Yang, L.; Li, X.; Zhang, X.; Huang, C. Supercritical solvothermal synthesis and formation mechanism of V_2O_3 microspheres with excellent catalytic activity on the thermal decomposition of ammonium perchlorate. *J. Alloys Compd.* **2019**, *806*, 1394–1402. [CrossRef]
10. Cheng, Z.; Chu, X.; Yin, J.; Dai, B.; Zhao, W.; Jiang, Y.; Xu, J.; Zhong, H.; Zhao, P.; Zhang, L. Formation of composite fuels by coating aluminum powder with a cobalt nanocatalyst: Enhanced heat release and catalytic performance. *Chem. Eng. J.* **2020**, *385*, 123859. [CrossRef]
11. Zhao, J.; Liu, Y.; Fu, X.C.; Deng, N.M. Cu/Carbon Aerogels Derived from HKUST-1 for the Thermal Decomposition of Ammonium Perchlorate. *ACS Appl. Nano Mater.* **2024**, *7*, 17373–17378. [CrossRef]
12. Lv, T.-T.; Xing, H.-Z.; Yang, H.-M.; Wang, H.-X.; Shi, J.; Cao, J.-P.; Lv, B.-L. Rapid synthesis of Cu_2O hollow spheres at low temperature and their catalytic performance for the decomposition of ammonium perchlorate. *CrystEngComm* **2021**, *23*, 7985–7993. [CrossRef]
13. Wei, S.; Zhang, Y.; Tan, H.; Xia, Z.; Zhai, L.; Hu, J.; Yang, Q.; Xie, G.; Chen, Z.; Chen, S. In Situ MOF-74-Pyrolysis-Generated Porous Carbon Supporting Spinel $Cu_{0.15}Co_{2.85}O_4$/C Boosts Ammonium Perchlorate Accelerating Decomposition: Precise Cu Doping Modulating Oxygen Vacancy Concentration. *Small* **2024**, *20*, 2400712. [CrossRef] [PubMed]
14. Ramdani, Y.; Liu, Q.; Huiquan, G.; Liu, P.; Zegaoui, A.; Wang, J. Synthesis and thermal behavior of Cu_2O flower-like, Cu_2O-C_{60} and Al/Cu_2O-C_{60} as catalysts on the thermal decomposition of ammonium perchlorate. *Vacuum* **2018**, *153*, 277–290. [CrossRef]
15. Tan, X.; Ding, C.; Wang, Y.; Chen, D.; Liang, T.; Meng, C.; Zhang, Y. Modulating electronic structure of cobalt silicate by iron-doping ensuring the boosted oxygen evolution reaction properties. *J. Colloid Interface Sci.* **2025**, *699*, 138168. [CrossRef]
16. Zhang, Y.; Tan, X.; Han, Z.; Wang, Y.; Jiang, H.; Zhang, F.; Zhu, X.; Meng, C.; Huang, C. Dual modification of cobalt silicate nanobelts by Co_3O_4 nanoparticles and phosphorization boosting oxygen evolution reaction properties. *J. Colloid Interface Sci.* **2025**, *679*, 1036–1045. [CrossRef]
17. Tang, X.; Zhou, P.; Zhou, Y.; Yuan, B.; Zhan, F.; Gao, J.; Liang, T.; Ren, Z.; Hu, M.; Zhang, Y.; et al. Structural design and evolution of one-dimensional Cu hydrogen-bonded organic framework for catalyzing the rapid decomposition of ammonium perchlorate. *J. Hazard. Mater.* **2025**, *486*, 136961. [CrossRef]
18. Lei, G.; Zhong, Y.; Xu, Y.; Yang, F.; Bai, J.; Li, Z.; Zhang, J.; Zhang, T. New Energetic Complexes as Catalysts for Ammonium Perchlorate Thermal Decomposition. *Chin. J. Chem.* **2021**, *39*, 1193–1198. [CrossRef]
19. Lv, T.-T.; Wang, H.-X.; Ren, X.-B.; Wang, L.-C.; Ding, R.-M.; Cao, J.-P.; Lv, B.-L. Protection of highly active sites on Cu_2O nanocages: An efficient crystalline catalyst for ammonium perchlorate decomposition. *CrystEngComm* **2020**, *22*, 8214–8220. [CrossRef]
20. Ji, H.; Fu, L.; Tan, S.; Zhang, Y.; Zhang, F.; Tang, X.; Jiang, W.; Li, X. CuO-ZnO heterojunction for enhanced catalytic decomposition of ammonium perchlorate via interfacial promotion. *J. Alloys Compd.* **2025**, *1044*, 184539. [CrossRef]
21. Liang, T.; Song, R.; Chen, C.; Alomar, T.S.; Xiao, F.; AlMasoud, N.; El-Bahy, Z.M.; Yang, Y.; Algadi, H.; Sun, L. Graphene oxide–supported Cu/Co nano-catalysts for thermal decomposition of ammonium perchlorate composites. *Adv. Compos. Hybrid Mater.* **2023**, *6*, 188. [CrossRef]
22. Li, S.; Li, M.; Han, J.; Xia, Z.; Chen, S.; Xie, G.; Gao, S.; Lu, J.Y.; Yang, Q. In situ growth of copper-based energetic complexes on GO and an MXene to synergistically promote the thermal decomposition of ammonium perchlorate. *Dalton Trans.* **2023**, *52*, 17458–17469. [CrossRef]
23. Xu, Y.; Wang, Y.; Zhong, Y.; Lei, G.; Li, Z.; Zhang, J.; Zhang, T. Transition Metal Complexes Based on Hypergolic Anions for Catalysis of Ammonium Perchlorate Thermal Decomposition. *Energy Fuels* **2020**, *34*, 14667–14675. [CrossRef]
24. Vipin Vijay, V.; Sajeev, L.B.; Anjana, S.; Balachandran, N.; Srinivas, C.; Vijayalekshmi, K.P.; Sreejith, K.J.; Devasia, R. "String and bead" model of copper modified polycarbosilane: Synthesis and applications. *J. Mater. Sci.* **2022**, *57*, 12393–12404. [CrossRef]
25. Gou, X.; Sun, X.; Yang, J.; Shi, J.; Yan, S.; Guo, X.; Yu, S.; Nie, J. Improvement of the Thermal Decomposition of Ammonium Perchlorate and Combustion of Aluminum Powder by Dual Core–Shell Ammonium Perchlorate-Based Composites Based on Self-Assembly Coating. *Langmuir* **2025**, *41*, 11674–11689. [CrossRef] [PubMed]

26. Cheng, Z.; Chu, X.; Xu, J.; Zhong, H.; Zhang, L. Synthesis of various CuO nanostructures via a Na3PO4–assisted hydrothermal route in a CuSO4–NaOH aqueous system and their catalytic performances. *Ceram. Int.* **2016**, *42*, 3876–3881. [CrossRef]
27. Luo, X.-L.; Wang, M.-J.; Yang, D.-S.; Yang, J.; Chen, Y.-S. Hydrothermal synthesis of morphology controllable Cu_2O and their catalysis in thermal decomposition of ammonium perchlorate. *J. Ind. Eng. Chem.* **2015**, *32*, 313–318. [CrossRef]
28. Luo, X.-L.; Wang, M.-J.; Yun, L.; Yang, J.; Chen, Y.-S. Structure-dependent activities of Cu_2O cubes in thermal decomposition of ammonium perchlorate. *J. Phys. Chem. Solids* **2016**, *90*, 1–6. [CrossRef]
29. Liu, Y.; Shao, Z.; Lv, T.; Zhang, Z.; Zhou, Z.; Hu, T.; Meng, C.; Zhang, Y. Conjugated polyaniline as "conveyor" in tungstate boosting cation storage for high-performance aqueous batteries. *Green Energy Environ.* **2025**, *10*, 766–779. [CrossRef]
30. Chen, J.; Hu, J.; Xiao, F. Fluorocarbon nanosheet@copper oxide microspheres: Simultaneous promotion the decomposition of ammonium perchlorate and ignition performance of aluminum. *J. Phys. Chem. Solids* **2023**, *172*, 111062. [CrossRef]
31. Zhou, X.; Xu, R.; Nie, H.; Yan, Q.; Liu, J.; Sun, Y. Insight into the precise catalytic mechanism of CuO on the decomposition and combustion of core–shell Al@AP particles. *Fuel* **2023**, *346*, 128294. [CrossRef]
32. Guo, Z.; Zhang, Q.; Liu, H.; Zhang, H.; Zhang, J.; Zuo, J.; Jin, B.; Peng, R. A novel metal-organic framework precursor strategy to fabricate sub-micron CuO microspheres for catalytic thermal decomposition of ammonium perchlorate. *Mater. Today Commun.* **2021**, *26*, 102139. [CrossRef]
33. Zheng, Z.; Zhou, P.; Tang, X.; Zeng, Q.; Yi, S.; Liao, J.; Hu, M.; Wu, D.; Zhang, B.; Liang, J.; et al. Hierarchical MOFs with Good Catalytic Properties and Structural Stability in Oxygen-Rich and High-Temperature Environments. *Small* **2024**, *20*, 2309302. [CrossRef] [PubMed]
34. Zhou, P.; Tang, X.; Ren, Z.; Zheng, Z.; Zhang, K.; Zhou, R.; Wu, D.; Liao, J.; Zhang, Y.; Huang, C. Oriented Assembled Prussian Blue Analogue Framework for Confined Catalytic Decomposition of Ammonium Perchlorate. *Small* **2023**, *19*, 2207023. [CrossRef] [PubMed]
35. Ji, H.; Tang, X.; Fu, L.; Li, J.; Zheng, Z.; Ding, C.; Zhang, Y.; Huang, C. Study on the Catalytic Effect of Nano Copper Oxide with Different Particle Sizes on the Thermal Decomposition of Ammonium Perchlorate. *Catalysts* **2025**, *15*, 882. [CrossRef]
36. Tang, X.; Zhao, J.; Yue, S.; Zhou, Y.; Yuan, B.; Zhou, P.; Ao, W.; Huang, C. Porous Cu_2O hierarchical structure for promoting the decomposition of ammonium perchlorate and its combustion properties. *Fuel* **2026**, *405*, 136781. [CrossRef]
37. ur Rehman, A.; Aadil, M.; Zulfiqar, S.; Agboola, P.O.; Shakir, I.; Aly Aboud, M.F.; Haider, S.; Warsi, M.F. Fabrication of binary metal doped CuO nanocatalyst and their application for the industrial effluents treatment. *Ceram. Int.* **2021**, *47*, 5929–5937. [CrossRef]
38. Du, Y.; Tang, Y.-T.; Ma, X.; Li, J.; Guo, Q. Design, Synthesis, and Diverse Applications of Cu-Based Photocatalysts: A Review. *Cryst. Growth Des.* **2024**, *24*, 2592–2618. [CrossRef]
39. Abdelhafiz, M.; Yehia, M.; Mostafa, H.E.; Wafy, T.Z. Catalytic action of carbon nanotubes on ammonium perchlorate thermal behavior. *React. Kinet. Mech. Catal.* **2020**, *131*, 353–366. [CrossRef]
40. Ozawa, T. Kinetic analysis of derivative curves in thermal analysis. *J. Therm. Anal.* **1970**, *2*, 301–324. [CrossRef]
41. Vyazovkin, S. Evaluation of activation energy of thermally stimulated solid-state reactions under arbitrary variation of temperature. *J. Comput. Chem.* **1997**, *18*, 393–402. [CrossRef]
42. Zhang, L.; Liu, Z.; Wang, X.; Heng, S.; Pan, Q.; Shao, Y.; Zhang, G.; Zhao, F. An Investigation on Fast Thermolysis of Ammonium Perchlorate (AP) by FTIR Spectroscopy. *Spectrosc. Spectr. Anal.* **2010**, *30*, 2098–2102.
43. Wang, X.; Wang, Q.; Wang, X.; Wang, J.; Zhang, G. Thermal pyrolysis properties and security performance of molecular perovskite energetic crystal $(C_6N_2H_{14})(NH_4)(ClO_4)_3$(DAP-4). *J. Anal. Appl. Pyrolysis* **2023**, *176*, 106268. [CrossRef]
44. Elbasuney, S.; Yehia, M. Thermal decomposition of ammonium perchlorate catalyzed with CuO nanoparticles. *Def. Technol.* **2019**, *15*, 868–874. [CrossRef]
45. Sivadas, D.L.; Thomas, D.; Haseena, M.S.; Jayalatha, T.; Krishnan, G.R.; Jacob, S.; Rajeev, R. Insight into the catalytic thermal decomposition mechanism of ammonium perchlorate. *J. Therm. Anal. Calorim.* **2019**, *138*, 1–10. [CrossRef]
46. Zhao, H.; Chen, M.; Zhu, X.; Chen, S.; Bian, Z. Cu(II) and Ni(II) complexes of ferrocene-containing unsaturated β-diketones: Electrochemical and burning-rate catalytic properties. *Res. Chem. Intermed.* **2013**, *41*, 3971–3980. [CrossRef]
47. Tzvetkov, G.; Spassov, T.; Tsvetkov, M.; Rangelova, V. Mesoporous cauliflower-like $CuO/Cu(OH)_2$ hierarchical structures as an excellent catalyst for ammonium perchlorate thermal decomposition. *Mater. Lett.* **2021**, *291*, 129534. [CrossRef]
48. Zhang, Y.; Li, Z.; Gao, F.; Ma, Z.; Li, W.; Gao, X.; Fan, G. Two amino acid Cu (II)-MOFs via one-pot method: Exhibiting good catalytic effect on the thermal decomposition of ammonium perchlorate and hexogen. *J. Solid State Chem.* **2022**, *316*, 123551. [CrossRef]

Disclaimer/Publisher's Note: The statements, opinions and data contained in all publications are solely those of the individual author(s) and contributor(s) and not of MDPI and/or the editor(s). MDPI and/or the editor(s) disclaim responsibility for any injury to people or property resulting from any ideas, methods, instructions or products referred to in the content.